

Thiolate-Bound Thulium Compounds: Synthesis, Structure, and NIR Emission

Santanu Banerjee,[†] G. Ajith Kumar,[‡] Thomas J. Emge,[†] Richard E. Riman,^{*,‡} and John G. Brennan^{*,†}

Department of Chemistry and Chemical Biology and Department of Ceramic & Material Engineering, Rutgers, the State University of New Jersey, 607 Taylor Road, Piscataway, New Jersey 08854-8087

Received March 4, 2008. Revised Manuscript Received April 17, 2008

Molecular (DME)₂Tm(SC₆F₅)₃ and tetrametallic (DME)₄(μ₂-SPh)₈Tm₄(SPh)₄ have been isolated in high yield and characterized by conventional methods. The fluorinated thiolate has an eight-coordinate Tm(III) ion bound to three sulfur atoms from the thiolates, four oxygen donors from the THF ligands, and a relatively weak dative Tm–F interaction with a 2.842(3) Å Tm–F separation. The benzenethiolate compound crystallizes as a tetramer with an alternating number (3, 2, 3) of thiolates connecting the nearly linear array of Tm(III) ions. Emission properties of both thiolates and the chalcogen-rich cluster (THF)₈Tm₄Se₉(SC₆F₅)₂ have been established. The Ph compound is significantly more emissive than either of the fluorinated species.

Introduction

An understanding of the variables that influence the lanthanide ion NIR emission intensity is important to the successful application of these ions in photonic materials.^{1–5} Chalcogen-based anions have been shown to provide a low-energy phonon environment that enhances the near IR emission intensity,⁵ and an extension of this work to molecular compounds has recently been described.^{6–12}

Improved intensity was first noted for the 1.54 μm emission from Er(III)^{6–9} in molecular (THF)₃Er(SC₆F₅)₃ and the heterochalcogen cluster (THF)₈Er₁₀S₆(SeSe)₆I₆, with quantum efficiencies (QE) that were significantly greater than QEs from any preceding molecular source. Subsequent investigations into analogous Nd compounds^{10–12} yielded equally dramatic results, with molecular (DME)₂Nd(SC₆F₅)₃ and the oxyselenido cluster (THF)₈Nd₈O₂Se₂(SePh)₁₄ not only emitting intensely at the technologically important 1.34 μm wavelength, but also displaying, for the first time, 1.8 μm emission from a molecular Nd source. This lower energy emission is found only with particularly low phonon energy solid-state materials, i.e., Nd₂Se₃ but not Nd₂O₃.¹³

In the development of polymer-based optical fiber technologies, there are three potentially useful lanthanides: Er, Nd, and Tm. Erbium's 1.5 μm emission arises out of the ⁴I_{13/2} → ⁴I_{15/2} transition and is currently employed in the telecommunication area because of the low attenuation of this energy by silica-based fiber optics.⁴ Nd³⁺ is more complicated, with a cascade of emission energies³ that are either rarely (1.34 μm) or, until recently (1.81 μm), never observed from molecular Nd³⁺ sources. Emission characteristics of the third source, Tm, are relatively unexplored, but the current application of Tm(III) as an eye-safe lasing ion in several hosts,¹⁴ coupled with the potential use of Tm materials in optical communications,¹⁴ as 0.82, 1.5, 1.8, and 2.34 μm lasers for optical sensing,¹⁵ metrology,¹⁶ and medicine,¹⁷ is stimulating interest in the chemical and physical properties of Tm(III) materials.

* Corresponding author. E-mail: bren@ccmail.rutgers.edu.

[†] Department of Chemistry and Chemical Biology, the State University of New Jersey.

[‡] Department of Ceramic & Material Engineering, Rutgers, the State University of New Jersey.

- (1) (a) Desurvire, E. *Sci. Am.* **1992**, *266*, 96. (b) Glass, A. M. *Phys. Today* **1993**, *46*, 34.
- (2) (a) Powell, R. C. *Physics of Solid State Laser Materials*; AIP Press: New York, 1998. (b) *Phosphor Handbook*; Shionoya, S., Yen, W. M., Eds.; CRC Press: Boca Raton, FL, 1999. (c) Sastri, V. C.; Bunzli, J. C.; Rao, V. R.; Rayudu, G. V. S.; Perumareddi, J. R. *Modern Aspects of Rare Earths and Their Complexes*; Elsevier: New York, 2003. (d) Reisfeld, R.; Jorgensen, C. K. *Lasers and Excited States of Rare Earths*; Springer Verlag, Berlin, 1977.
- (3) Kaminskii, A. A. *Laser Crystals Their Physics and Properties*; Springer Verlag: Berlin, 1981.
- (4) Becker, P. C.; Olsson, N. A.; Simpson, J. R. *Erbium-Doped Fiber Amplifiers—Fundamentals and Technology*; Academic Press: New York, 1999.
- (5) (a) Yang, P.; Meng, K. L.; Song, C. F.; Zhou, G. J.; Xu, D.; Yuan, D. R. *Inorg. Chem. Commun.* **2002**, *5*, 187. (b) Kasap, S. O.; Koughia, K.; Munzar, M.; Tonchev, D.; Saitou, D.; Aoki, T. *J. Non-Cryst. Solids* **2007**, *353*, 1364. (c) Reisfeld, R. *Struct. Bonding (Berlin)* **2004**, *106*, 209.
- (6) Kornienko, A.; Kumar, G. A.; Riman, R. E.; Emge, T. J.; Brennan, J. G. *J. Am. Chem. Soc.* **2005**, *127*, 3501.
- (7) Kumar, G. A.; Kornienko, A.; Banerjee, S.; Riman, R. E.; Emge, T. J.; Brennan, J. G. *Chem. Mater.* **2005**, *17*, 5130.
- (8) Kumar, G. A.; Riman, R. E.; Chen, S.; Smith, D.; Ballato, J.; Banerjee, S.; Kornienko, A.; Brennan, J. G. *Appl. Phys. Lett.* **2006**, *88*, 91902.
- (9) Kornienko, A.; Banerjee, S.; Kumar, G. A.; Riman, R. E.; Emge, T. J.; Brennan, J. G. *J. Am. Chem. Soc.* **2005**, *127*, 14008.
- (10) Banerjee, S.; Kumar, G. A.; Riman, R. E.; Emge, T. J.; Brennan, J. G. *J. Am. Chem. Soc.* **2007**, *129*, 5926.
- (11) Kumar, G. A.; Riman, R. E.; Diaz Torres, L. A.; Banerjee, S.; Romanelli, M. D.; Emge, T. J.; Brennan, J. G. *Chem. Mater.* **2007**, *19*, 2937.
- (12) Banerjee, S.; Huebner, L.; Romanelli, M. D.; Kumar, G. A.; Riman, R. E.; Emge, T. J.; Brennan, J. G. *J. Am. Chem. Soc.* **2005**, *127*, 15900.

(13) Hasegawa, Y.; Murakoshi, K.; Wada, Y.; Kim, J. H.; Nakashima, N.; Yamanaka, T.; Yanagida, S. *Chem. Phys. Lett.* **1996**, *248*, 8.

(14) *Rare Earth Doped Fiber Lasers and Amplifiers*; Dignonnet, M. J. F., Ed.; Marcel Dekker: New York, 1993.

(15) Jha, A. *Proc. SPIE* **2006**, *6409*, 640918.

(16) Sokólska, I.; Ryba-Romanowski, W.; Golab, S.; Baba, M.; Wirkowicz, M.; Ukasiewicz, T. *J. Phys. Chem. Solids* **2000**, *61*, 1573.

(17) de Camargo, A. S. S.; Nunes, L. A. O.; Botero, E. R.; Garcia, D.; Eiras, J. A. *Chem. Phys. Lett.* **2005**, *410*, 156.

In this paper, we continue our investigation into the emissive properties of chalcogen bound Ln ions. A pair of Tm thiolate compounds, $(\text{DME})_2\text{Tm}(\text{SC}_6\text{F}_5)_3$ and $(\text{DME})_4(\mu_2\text{-SPh})_8\text{Tm}_4(\text{SC}_6\text{H}_5)_4$, were prepared along with the previously described Tm cluster $(\text{THF})_6\text{Tm}_4\text{Se}_9(\text{SeC}_6\text{F}_5)_2$,¹⁸ in order to examine how chalcogen-based anions influence Tm emission and evaluate the effect of chalcogenolate fluorination upon Tm NIR emission intensity.

Experimental Section

General Methods. All syntheses were carried out under ultra pure nitrogen (WELCO CGI, Pine Brook, NJ), using conventional dry box or Schlenk techniques. Solvents (Fisher Scientific, Agawam, MA) were purified with a dual-column Solv-Tek solvent purification system (Solv-Tek Inc., Berryville, VA). Tm and Hg were purchased from Strem Chemicals (Newburyport, MA). HSC_6F_5 was purchased from Aldrich. Anhydrous pyridine (Aldrich Chemicals, Milwaukee, WI) was purchased and refluxed over KOH (Aldrich). $(\text{THF})_6\text{-Tm}_4\text{Se}_9(\text{SeC}_6\text{F}_5)_2$ was prepared according to literature procedure.¹⁸ Melting points were taken in sealed capillaries and are uncorrected. IR spectra were taken on a Thermo Nicolet Avatar 360 FTIR spectrometer and recorded from 4000 to 600 cm^{-1} as a Nujol mull on NaCl plates. Elemental analyses were performed by Quantitative Technologies, Inc. (Whitehouse Station, NJ).

Synthesis of $(\text{DME})_2\text{Tm}(\text{SC}_6\text{F}_5)_3$ (1). Tm (0.186 g, 1.10 mmol) and $\text{Hg}(\text{SC}_6\text{F}_5)_2$ (0.987 g, 1.65 mmol) were combined in DME (30 mL), and the mixture was stirred until the pieces of metal were dissolved completely and elemental mercury was visible in the bottom of the flask (overnight). The very pale yellow solution was decanted to separate the mercury (0.28 g, 86%) and filtered, reduced in volume under a vacuum to ca. 15 mL, and layered with hexane (15 mL) to give pale yellow crystals (0.85 g, 72%) which turn opaque white at 91 °C, melt at 212 °C, begin to darken at 297 °C, and continue to darken up to 350 °C. Anal. Calcd for $\text{C}_{26}\text{H}_{20}\text{F}_{15}\text{O}_4\text{S}_3\text{Tm}$: C, 33.0; H, 2.11. Found: C, 33.4; H, 2.22. IR: 2921 (s), 2855 (s), 1509 (m), 1470 (s), 1382 (m), 1263 (m), 1192 (w), 1082 (m), 1077 (m), 1035 (m), 985 (w), 971 (m), 910 (w), 871 (m), 863 (m), 848 (m), 799 (w), 719 (w) cm^{-1} .

Synthesis of $(\text{DME})_4(\mu_2\text{-SPh})_8\text{Tm}_4(\text{SPh})_4$ (2). Tm (0.17 g, 1.0 mmol) and $(\text{SPh})_2$ (0.33 g, 1.5 mmol) were combined in DME (40 mL) in presence of catalytic Hg (0.03 g, 0.15 mmol). The reaction mixture was stirred until the pieces of metal were dissolved completely (5 days). The straw yellow colored solution was filtered away from a trace amount of black powdery precipitate at the bottom of the flask. The filtrate was reduced in volume under vacuum to ca. 15 mL and layered with hexane (15 mL). After one week light yellow colored, block shaped crystals (0.21 g, 43%) appeared. The crystals turn white at 102 °C, melt at 223 °C, and continue to darken up to 350 °C. Anal. Calcd. for $\text{C}_{88}\text{H}_{100}\text{Tm}_4\text{O}_8\text{S}_{12}$: C, 45.1; H, 4.27. Found: C, 45.6; H, 4.43. IR: 2927 (s), 2854 (m), 1945 (m), 1862 (s), 1637 (s), 1582 (m), 1458 (m), 1380 (s), 1259 (s), 1222 (s), 1148 (s), 1072 (s), 1034 (s), 898 (m), 811 (m), 740 (m), 702 (m), 605 (m), 487 (m), 418 (m) cm^{-1} .

X-ray Structure Determination. Data for **1** and **2** were collected on a Bruker Smart APEX CCD diffractometer with graphite monochromatized Mo $\text{K}\alpha$ radiation ($\lambda = 0.71073\text{\AA}$) at 100 K. Crystals were immersed in Paratone oil and examined at low temperatures. The data were corrected for Lorentz effects and polarization, and absorption, the latter by a multiscan (SADABS)¹⁹ method. The structure was solved by

Table 1. Summary of Crystallographic Details for **1** and **2**^a

| | 1 | 2 |
|--|--|---|
| empirical formula | $\text{C}_{26}\text{H}_{20}\text{F}_{15}\text{O}_4\text{S}_3\text{Tm}$ | $\text{C}_{88}\text{H}_{100}\text{O}_8\text{S}_{12}\text{Tm}_4$ |
| fw | 946.53 | 2346.12 |
| space group | $P2_12_12_1$ | $P2_1/n$ |
| <i>a</i> (Å) | 8.5102(10) | 21.093(17) |
| <i>b</i> (Å) | 24.246(3) | 18.8259(15) |
| <i>c</i> (Å) | 30.449(3) | 23.6882(19) |
| β (deg) | | 98.347(2) |
| <i>V</i> (Å ³) | 6276.2(12) | 9306.9 |
| <i>Z</i> | 8 | 4 |
| <i>D</i> _{calcd} (g/cm ⁻³) | 2.003 | 1.674 |
| <i>T</i> (K) | 100(2) | 100(2) |
| λ (Å) | 0.71073 | 0.71073 |
| abs coeff (mm ⁻¹) | 3.150 | 4.097 |
| <i>R</i> (<i>F</i>) ^b [<i>I</i> > 2σ(<i>I</i>)] | 0.0308 | 0.0436 |
| <i>R</i> _w (<i>F</i>) ^c [<i>I</i> > 2σ(<i>I</i>)] | 0.0725 | 0.0881 |

^a Additional crystallographic details are given in the Supporting Information. ^b $R(F) = \sum ||F_o| - |F_c|| / \sum |F_o|$. ^c $R_w(F^2) = \{\sum [w(F_o^2 - F_c^2)^2] / \sum [w(F_o^2)^2]\}^{1/2}$.

direct methods (SHELXS86).²⁰ All non-hydrogen atoms were refined (SHELXL97)²¹ based on F_{obs}^2 . All hydrogen atom coordinates were calculated with idealized geometries (SHELXL97). Scattering factors (f_o , f' , f'') are as described in SHELXL97. Crystallographic data and final *R* indices for **1** and **2** are given in Table 1. ORTEP diagrams^{22,23} for **1** and **2** are shown in Figures 1 and 2, respectively. Significant bond distances are given in the figure captions. Complete crystallographic details for **1** and **2** are given in the Supporting Information.

Spectroscopy. Absorption measurements were carried out with crystalline powder dissolved in THF using a double beam spectrophotometer (Perkin-Elmer Lambda 9, Wellesley, MA) in a 1 cm cuvette using THF as the reference solvent. The emission spectra of the powdered samples were recorded by exciting the sample with the 800 nm band of a Ti:S-laser. The emission from the sample was focused onto a 0.55 m monochromator (Jobin Yvon, Triax 550, Edison, NJ) and detected by a thermoelectrically cooled InGaAs detector. The signal was intensified with a lock-in amplifier (SR 850 DSP, Stanford Research System, Sunnyvale, CA) and processed with a computer controlled by the Spectramax commercial software (GRAMS 32, Galactic Corp, Salem, New Hampshire). To measure the decay time, the laser beam was modulated by a chopper and the signal was collected on a digital oscilloscope (Model 54520A, 500 MHz, Hewlett-Packard, Palo Alto, CA).

Emission Data Analysis. The radiative lifetime (τ_{rad}) of the infrared emitting state is related to the total spontaneous emission probability of all the transitions from an excited-state by $\tau_{\text{rad}} = (\sum A_{J'J})^{-1}$ where *A* is calculated using Judd–Ofelt theory^{24,25} as

$$A_{\text{rad}}(i \rightarrow j) = \frac{64\pi^4}{3h(2J+1)e^2\lambda^3} \left[\frac{n(n^2+2)^2}{9} \right] \sum_{i=2,4,6} \Omega_i \langle \psi || U^i || \psi' \rangle^2 \quad (1)$$

Where *n* is the refractive index, Ω_i are the Judd–Ofelt intensity parameters, and $\|U^i\|$ are doubly reduced matrix elements operators corresponding to the $J \rightarrow J'$ transition. The three Judd–Ofelt parameters were obtained by fitting the measured oscillator strength to the theoretical oscillator strength using the least-squares tech-

(20) Sheldrick, G. M. *SHELXS86, Program for the Solution of Crystal Structures*; University of Göttingen: Göttingen, Germany, 1986.

(21) Sheldrick, G. M. *SHELXL97, Program for Crystal Structure Refinement*, University of Göttingen: Göttingen, Germany, 1997.

(22) Johnson, C. K.; *ORTEP II*; Report ORNL-5138; Oak Ridge National Laboratory: Oak Ridge, TN, 1976.

(23) Sheldrick, G. M. *SHELXTL (XP)*, version 6.14; Bruker-AXS: Madison, WI, 2000.

(18) Fitzgerald, M.; Emge, T. J.; Brennan, J. G. *Inorg. Chem.* **2002**, *41*, 3528.

(19) SADABS, Bruker Nonius Area Detector Scaling and Absorption Correction, version 2.05; Bruker-AXS: Madison, WI, 2003.

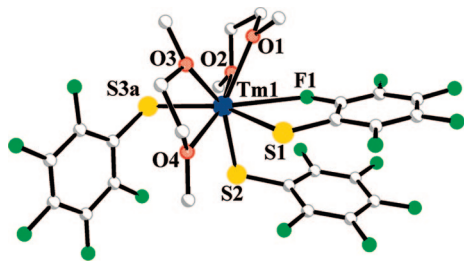


Figure 1. ORTEP diagram of $(\text{DME})_2\text{Tm}(\text{SC}_6\text{F}_5)_3$, with blue, Tm; yellow, S; red, O; green, F; white, C; and with the H atoms removed for clarity. Significant distances (Å): Tm(1)–O(1), 2.385(3); Tm(1)–O(2), 2.406(3); Tm(1)–O(4), 2.416(3); Tm(1)–O(3), 2.419(4); Tm(1)–S(3A), 2.707(1); Tm(1)–S(3B), 2.707(1); Tm(1)–S(1), 2.716(1); Tm(1)–S(2), 2.721(1); Tm(1)–F(1), 2.840(3).

nique. The quality of the fit is determined by the rms deviation between the experimental and theoretical values of the dipole strengths obtained from the expression

$$\text{RMS} = \sqrt{\frac{\sum (\Delta S)^2}{(N - m)}} \quad (2)$$

Where ΔS is the difference between the experimental and calculated dipole strengths, N the number of transitions, and m the number of fitting parameters.

The stimulated emission cross-section of the emission band is obtained with the help of the Fuchtbauer–Ladensburg equation³

$$\sigma_{\text{em}} = \frac{\lambda^4 A}{8\pi c n^2 \Delta\lambda_{\text{eff}}} \quad (3)$$

where $\Delta\lambda_{\text{eff}}$ is the effective line-width of the emission band obtained by integrating over the entire emission band and dividing by the peak fluorescence intensity. The lifetime of the emission band is extracted from the decay curve by the curve fitting option of the ORIGIN software.

Results and Discussion

Molecular DME complexes of both $\text{Tm}(\text{SC}_6\text{F}_5)_3$ and $\text{Tm}(\text{SC}_6\text{H}_5)_3$ can be isolated in crystalline form. The fluorinated thiolate crystallizes as monomeric $(\text{DME})_2\text{Tm}(\text{SC}_6\text{F}_5)_3$ (**1**), with two chelating DME ligands, three terminal thiolates, and a dative Tm–F interaction with a 2.842(3) Å Tm–F separation defining an eight coordinate structure. An ORTEP diagram of the molecular structure of one of the two crystallographically independent molecules within the unit cell of **1** is shown in Figure 1, with significant bond distances shown in the caption. The Tm^{3+} ionic concentration in the unit cell is 1.27×10^{21} ions/cm³, which is higher than the typical concentrations of rare earth doped materials (ca. $\sim 1 \times 10^{18}$ to 1×10^{19} ions/cm³).

In contrast, the analogous benzenethiolate crystallizes as tetrametallic $(\text{DME})_4(\mu_2\text{-SPh})_8\text{Tm}_4(\text{SPh})_4$ (**2**). An ORTEP diagram showing the molecular structure of **2** is shown in Figure 2 with significant bond distances shown in the caption. In **2** there is a nearly linear array of Tm(III) ions connected with an alternating series of 3–2–3 μ_2 thiolate ligands. Each Tm coordinates a chelating DME ligand, and there are two terminal thiolate anions coordinating to the outer Tm(III) ions such that all four Tm are seven coordinate. Tm–S bond lengths to the terminal thiolate ligands are shorter than bond

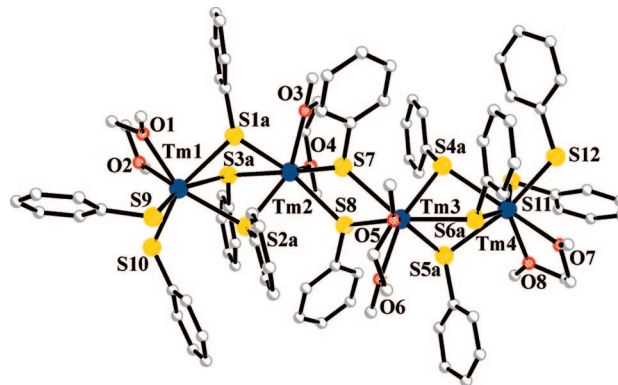


Figure 2. ORTEP diagram of $(\text{DME})_4(\mu_2\text{-SPh})_8\text{Tm}_4(\text{SPh})_4$, with blue, Tm; yellow, S; red, O; white, C; and with the H atoms removed for clarity. Significant distances (Å): Tm(1)–O(1), 2.396(3); Tm(1)–O(2), 2.442(3); Tm(1)–S(9), 2.6535(11); Tm(1)–S(10), 2.7054(13); Tm(1)–S(1B), 2.726(6); Tm(1)–S(2A), 2.7841(13); Tm(1)–S(3A), 2.7862(14); Tm(1)–S(2B), 2.791(7); Tm(1)–S(1A), 2.8356(13); Tm(1)–S(3B), 2.853(7); Tm(2)–O(4), 2.358(3); Tm(2)–O(3), 2.362(3); Tm(2)–S(3B), 2.710(7); Tm(2)–S(3A), 2.7241(13); Tm(2)–S(7), 2.7257(12); Tm(2)–S(1B), 2.738(6); Tm(2)–S(1A), 2.7559(13); Tm(2)–S(2A), 2.7566(13); Tm(2)–S(8), 2.7643(12); Tm(2)–S(2B), 2.784(7); Tm(3)–O(6), 2.314(3); Tm(3)–O(5), 2.407(3); Tm(3)–S(6B), 2.655(4); Tm(3)–S(7), 2.7280(12); Tm(3)–S(5A), 2.7432(15); Tm(3)–S(6A), 2.7434(15); Tm(3)–S(8), 2.7577(12); Tm(3)–S(4B), 2.761(4); Tm(3)–S(5B), 2.766(4); Tm(3)–S(4A), 2.7702(15); Tm(4)–O(8), 2.393(3); Tm(4)–O(7), 2.471(3); Tm(4)–S(11), 2.6458(13); Tm(4)–S(12), 2.6958(12); Tm(4)–S(4B), 2.750(4); Tm(4)–S(6A), 2.7513(16); Tm(4)–S(4A), 2.7928(15); Tm(4)–S(5B), 2.821(4); Tm(4)–S(5A), 2.8240(15); Tm(4)–S(6B), 2.863(4).

lengths to the bridging ligands, as has been noted in pyridine coordination polymers of the earlier lanthanides. The concentration of Tm(III) in crystalline **2** is 1.72×10^{21} ions/cm³. The slightly higher density of Tm ions in **2** versus that of **1** contrasts the lower crystalline density of the former, due to its greater overall van der Waals interaction volume by means of its larger extended array of SPh ligands. While there have been a number of coordination compounds reported for lanthanide benzenethiolates, this is the first example where the less-polar DME ligand was able to coordinate to a Ln(III) ion and deliver a soluble/crystalline product. Previous Ln(SPh)₃ complexes include the monometallic complexes $(\text{HMPA})_3\text{Sm}(\text{SPh})_3$ ²⁶ and $(\text{py})_3\text{Yb}(\text{SPh})_3$ ²⁷ dimeric $[(\text{py})_3\text{Tm}(\text{SPh})_3]_2$, and polymeric $([(\text{THF})\text{Sm}(\text{SPh})_3]_n)$ ²⁸ Variations in structure have been rationalized in terms of relative Lewis basicity and the tendency of thiolates to bridge larger lanthanides while bonding in a terminal fashion to the latter metals in the series. The fact that **1** is monometallic and **2** is a tetramer can be explained in terms of basicity at the sulfur donor, with the fluoride substituents in **1** polarizing electron density away from the sulfur atom, rendering it less electron rich and thus less able to compete with oxygen donors for access to the cation coordination sphere. Fluorinated thiolates have rarely formed multimetallic structures, with no more than dimers forming

(24) Judd, B. R. *Phys. Rev. B* **1962**, *127*, 750.

(25) Ofelt, G. S. *J. Chem. Phys.* **1962**, *37*, 511.

(26) Mashima, K.; Nakayama, Y.; Shibahara, T.; Fukumoto, H.; Nakamura, A. *Inorg. Chem.* **1996**, *35*, 93.

(27) Lee, J.; Brewer, M.; Berardini, M.; Brennan, J. G. *Inorg. Chem.* **1995**, *34*, 3215.

(28) Lee, J.; Freedman, D.; Melman, J. H.; Brewer, M.; Sun, L.; Emge, T. J.; Long, F. H.; Brennan, J. G. *Inorg. Chem.* **1998**, *37*, 2512.

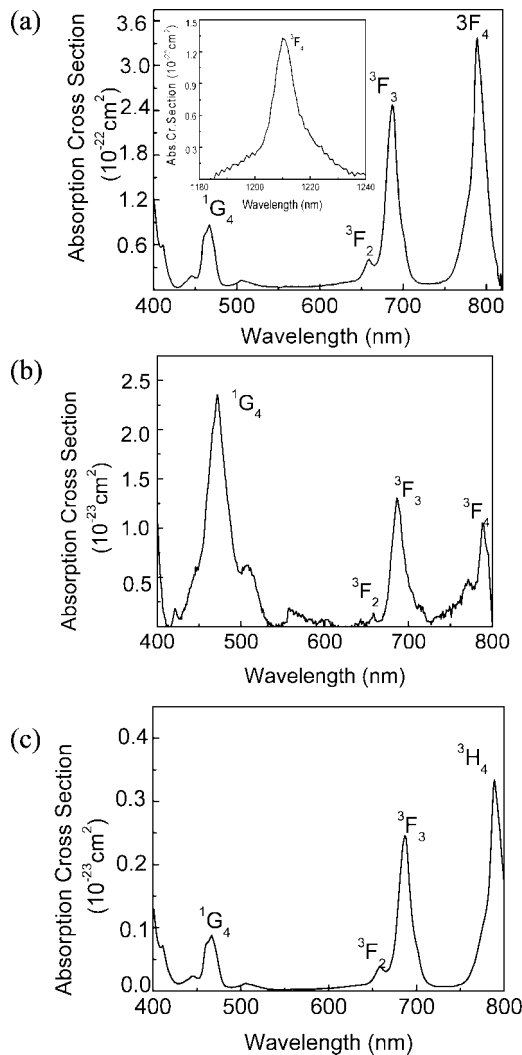


Figure 3. Absorption spectrum of (a) $(\text{DME})_2\text{Tm}(\text{SC}_6\text{F}_5)_3$, (b) $(\text{DME})_4\text{Tm}_4(\text{SPH})_{12}$, and (c) $(\text{THF})_6\text{Tm}_4\text{Se}_9(\text{SeC}_6\text{F}_5)_2$ in THF at 0.023 mmol concentration with the spectroscopic notations for the observed band transitions. The inset of (a) shows the ${}^3\text{H}_6 \rightarrow {}^3\text{F}_4$ transition.

in trivalent chemistry, and the one exception being a polymeric structure forming with divalent Eu.^{29,30}

The previously reported chalcogen-rich cluster $(\text{THF})_6\text{Tm}_4\text{Se}_9(\text{SC}_6\text{F}_5)_2$ (**3**) contains a square array of Tm(III) ions connected by a central $\mu_4\text{Se}^{2-}$, with $(\text{SeSe})^{2-}$ ligands bridging adjacent Tm ions that have an average 4.1 Å Tm–Tm separation.¹⁸ The compound crystallizes in the triclinic space group $P\bar{1}$, and has an ion concentration of 2.617×10^{21} ions/cm³.

The room temperature absorption spectra for **1**, **2**, and **3** are shown in Figure 3a–c. In the 400–800 nm region, four $f \rightarrow f$ absorption bands of Tm^{3+} are observed that originate from the ${}^3\text{H}_6$ ground-state to various excited states. In **2**, an additional band is observed at 1212 nm, which corresponds to the ${}^3\text{H}_6 \rightarrow {}^3\text{F}_4$ transition. All absorption bands are identified using the standard notations as shown in Figure

Table 2. Observed Absorption Band Transitions with Their Band Positions, Oscillator Strength and Calculated Judd–Ofelt Parameters^a

| transition from ${}^3\text{H}_6$ to | wavelength (nm) | | | $f (\times 10^{-6})$ | | | | | |
|-------------------------------------|-----------------|------|------|----------------------|-------|------|------|-------|-------|
| | 1 | 2 | 3 | 1 | | 2 | | 3 | |
| | exp | cal | exp | exp | cal | exp | cal | exp | cal |
| ${}^1\text{G}_4$ | 471 | 467 | 464 | 0.08 | 0.072 | 0.24 | 0.3 | 0.242 | 0.031 |
| ${}^3\text{F}_2$ | | 656 | | | | 0.07 | 0.04 | 0.063 | 0.072 |
| ${}^3\text{F}_3$ | 686 | 685 | 689 | 0.0147 | 0.031 | 0.26 | 0.31 | 0.083 | 0.072 |
| ${}^3\text{H}_4$ | 789 | 788 | 792 | 0.01 | 0.023 | 0.32 | 0.52 | 0.018 | 0.009 |
| ${}^3\text{H}_5$ | 1135 | 1136 | 1132 | 0.37 | 0.013 | 0.43 | 0.61 | 0.183 | 0.191 |

| Ω parameters ($\times 10^{-20} \text{cm}^2$) for 1 | | |
|--|------------|------------|
| Ω_2 | Ω_4 | Ω_6 |
| 0.6 | 1 | 0.03 |
| | 0.04 | |
| | 2 | |
| 2 | 0.03 | 0.2 |
| | 3 | |
| | 0.05 | |
| 1.2 | 0.05 | 0.04 |

^a RMS(1) = 0.357×10^{-6} , RMS(2) = 0.191×10^{-6} , RMS(3) = 0.151×10^{-6} . Ionic concentrations (N): **1** = 1.274×10^{21} ions/cc, **2** = 1.719×10^{21} ions/cc, **3** = 2.617×10^{21} ions/cc.

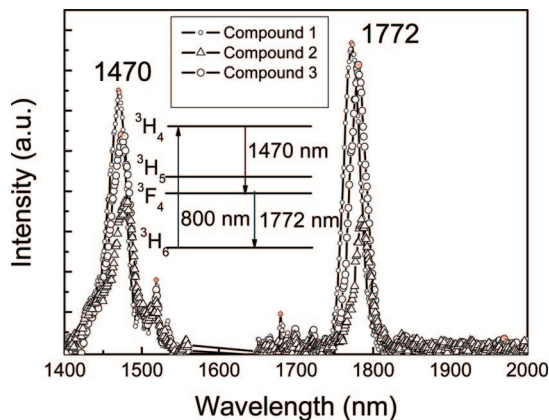


Figure 4. Comparison of the emission spectra of Tm^{3+} in the three complexes with the pumping scheme and emission channels in the inset.

3. The absorption cross-sections of **1** and **3** are an order of magnitude smaller than **2**. All are significantly lower than the cross-sections for Tm-doped sulfide glass.^{31,32}

All of the observed absorption bands were numerically integrated to obtain the experimental oscillator strength and the values obtained are summarized in Table 2a along with the observed band positions and their spectral assignments. The measured oscillator strengths (f_{exp}) were fitted with calculated oscillator strength (f_{cal}) values to obtain the three phenomenological intensity parameters. For **1**, these are $\Omega_2 = 0.6 \times 10^{-20} \text{cm}^2$, $\Omega_4 = 0.04 \times 10^{-20} \text{cm}^2$, and $\Omega_6 = 10.03 \times 10^{-20} \text{cm}^2$. For **2**, the corresponding values are $\Omega_2 = 2.0 \times 10^{-20} \text{cm}^2$, $\Omega_4 = 0.03 \times 10^{-20} \text{cm}^2$, and $\Omega_6 = 0.2 \times 10^{-20} \text{cm}^2$, respectively. For **3**, the values are $\mu_2 = 1.2 \times 10^{-20} \text{cm}^2$, $\mu_4 = 0.05 \times 10^{-20} \text{cm}^2$, and $\mu_6 = 0.04 \times 10^{-20} \text{cm}^2$, respectively. Associated rms values were found to be on the order of $0.198\text{--}0.357 \times 10^{-6} \text{cm}^2$, proving that the

(29) Melman, J.; Emge, T. J.; Brennan, J. G. *Inorg. Chem.* **2001**, *40*, 1078.

(30) Melman, J.; Rhode, C.; Emge, T. J.; Brennan, J. G. *Inorg. Chem.* **2002**, *41*, 28.

(31) Yang, Z.; Luo, Lan.; Chen, Wei. *J. Appl. Phys.* **2006**, *076107*, 99.

(32) Truong, V. G.; Jurdyc, A. M.; Jacquier, B.; Ham, B. S.; Quang, A. Q. L.; Leperson, J.; Nazabal, V.; Adam, J. L. *J. Opt. Soc. Am. B* **2006**, *2588*, 23.

Table 3. Measured and Calculated Decay Times of the Observed Emission Transitions with the Radiative Quantum Efficiencies

| transition | radiative decay time (τ_{rad} , μs) | | | fluorescence decay time (τ_{fl} , μs) | | | quantum efficiency ($\eta\%$) | | |
|---|--|-------|-------|--|-----|-----|---------------------------------|------|-------|
| | 1 | 2 | 3 | 1 | 2 | 3 | 1 | 2 | 3 |
| $^3\text{H}_4 \rightarrow ^3\text{F}_4$ | 3195 | 996 | 1661 | 70 | 111 | 80 | 2.2 | 11.1 | 4.8 |
| $^3\text{F}_4 \rightarrow ^3\text{H}_6$ | 67796 | 18726 | 35714 | 80 | 120 | 110 | 0.118 | 0.64 | 0.308 |

Judd–Ofelt model is suitable for predicting the radiative spectral properties with three fitting parameters. The calculated intensity parameters were used to evaluate the transition probability and radiative decay time for the infrared bands of interest.

The fluorescence spectra of **1**, **2**, and **3** are shown in Figure 4. Two major emission bands are observed at 1470 and 1772 nm with effective bandwidths of 38 and 27 nm in **1**; 51 and 29 nm in **2**; 34 and 22 nm in **3**. The excitation and de-excitation scheme in Tm^{3+} is shown in the inset of Figure 4. Upon excitation of the level $^3\text{H}_4$ a fraction of the population was de-excited to $^3\text{F}_4$, giving rise to the 1.4 μm transition, with the remaining excited-state population relaxing through the channel $^3\text{F}_4 \rightarrow ^3\text{H}_6$ via 1.7 μm emission.

To understand the stimulated emission properties of these emission bands the values radiative lifetime (τ_{rad}) were calculated using the Judd–Ofelt parameters and are summarized in Table 3. The room temperature fluorescence decay curves obtained for the two emission bands of **1**, **2**, and **3** are shown in Figures 5–7, respectively. To measure the quantum efficiencies of the emission bands, the fluorescence decay time (τ_{fl}) was extracted from the measured decay curve. Both decay curves were curve fitted with ORIGIN software to yield decay times of 70 and 80 μs in **1**; 111 and 120 μs in **2**; and 80 and 110 μs in **3** for the 1.4 and 1.7 μm bands. Because the radiative decay time is inversely proportional to the linear combination of Ω_2 , Ω_4 , and Ω_6 , the

lower Ω values in **1** yield higher radiative decay times for both emission bands in **1**. The experimental decay time, together with the calculated radiative decay time results in calculated quantum efficiencies for the 1.4 μm band of 2.2, 11.1, and 4.8%, for **1**, **2**, and **3**, respectively, whereas for the 1.7 μm band, the efficiency is too low, in the range of 0.11 to 0.64%. Even though these values are several times shorter compared to inorganic materials, we believe that these values are the highest reported efficiencies for molecular Tm^{3+} compounds.

The NIR emission properties of molecular Tm compounds are relatively unexplored. Earlier, Alexey et al.³³ reported the spectroscopic properties of Tm(III) tris β -diketonates for the $^3\text{H}_4 \rightarrow ^3\text{H}_6$ emission band at 800 nm. The reported lifetime was in the range of 5–25 μs with a maximum quantum efficiency of 1%. The lower quantum efficiencies in these complexes relative to **1–3** can be rationalized in terms of the higher energy transfer induced concentration quenching as well as being due to the additional de-excitation path through to the triplet states of the ligand, which are lying close to the excitation levels. NIR emission from Tm imino nitroxide³⁴ and dibenzolylmethanato³⁵ compounds have also been noted, but quantum efficiencies were not obtained from these studies.

For all compounds, the quantum efficiency of the $^3\text{H}_4$ level is higher than that of the $^3\text{F}_4$ or $^3\text{H}_5$ because of the difference in the difference in the energy gap participating in the emission transitions and the associated multiphonon relaxation rates. The energy gap of $^3\text{H}_5 \rightarrow ^3\text{F}_4$ is about 2580 cm^{-1} and that of $^3\text{H}_4 \rightarrow ^3\text{F}_4$ is about 4260 cm^{-1} . Assuming a vibrational frequency of 350 cm^{-1} for the host, seven and twelve phonons are required to undergo multiphonon relaxation. Because the probability of multiphonon relaxation increases with the decrease in energy gap the multiphonon decay rate is more prominent for the transitions originating from the $^3\text{H}_5$ level, which decays to $^3\text{F}_4$. The quantum efficiency of the fluorinated compounds are significantly lower than the benzenethiolate, even though there are fewer C–H bonds present in the ether donor ligands of the latter, and so the improvement can be attributed to the fluorination of the thiolate ring. In contrast the $^3\text{H}_4$ level is unaffected by multiphonon decay and emits with high quantum yield as observed.

Assuming a Gaussian line shape the stimulated emission cross sections of the emission transitions are evaluated using eq 3. According to eq 3, the calculated emission cross-section of the 1.4 μm band is $2.26 \times 10^{-20} \text{ cm}^2$ for **1**, $5.58 \times 10^{-20} \text{ cm}^2$ for

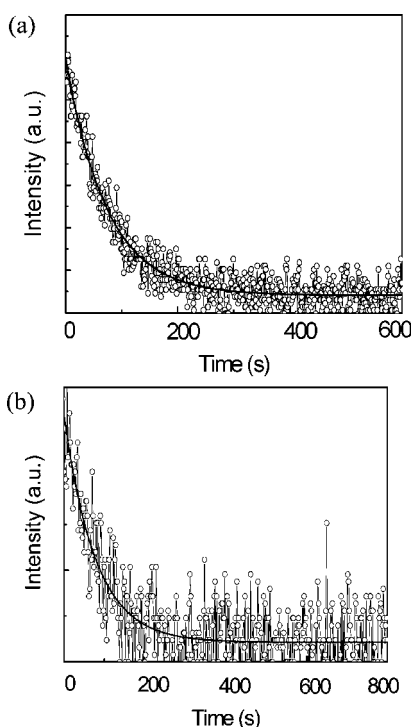


Figure 5. Fluorescence decay curves of the (a) 1.4 and (b) 1.7 μm emissions in $(\text{DME})_2\text{Tm}(\text{SC}_6\text{F}_5)_3$.

- (33) Alexey, V. T.; Carpenter, A. V.; Gorokhovskiy, A. A.; Alfano, R. R.; Chu, T. Y.; Okamoto, Y. *Proc. SPIE* **1998**, *165*, 3468.
 (34) Kaizaki, S.; Shirotani, D.; Tsukahara, Y.; Nakata, H. *Eur. J. Inorg. Chem.* **2005**, *1*, 3503.
 (35) Zang, F. X.; Hong, Z. R.; Li, W. L.; Li, M. T.; Sun, X. Y. *Appl. Phys. Lett.* **2004**, *84*, 2679.

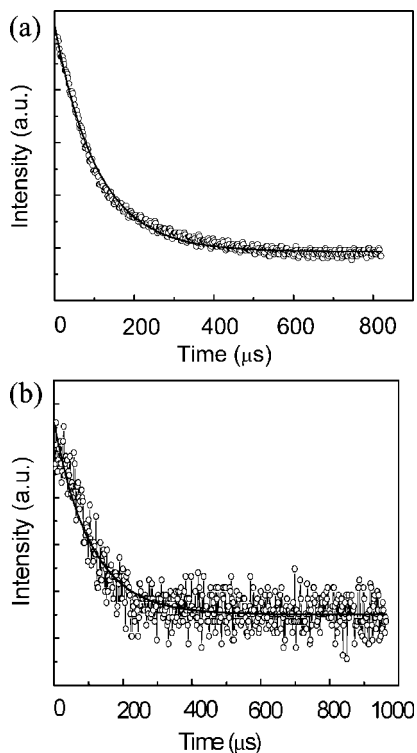


Figure 6. Fluorescence decay curves of the (a) 1.4 and (b) 1.7 μm emissions in $(\text{DME})_4\text{Tm}_4(\text{SPh})_{12}$.

2, and $2.02 \times 10^{-20} \text{ cm}^2$ for **3**, whereas for the 1.7 μm band, the emission cross-sections are $0.317 \times 10^{-20} \text{ cm}^2$ for **1**, $1.08 \times 10^{-20} \text{ cm}^2$ for **2**, and $0.25 \times 10^{-20} \text{ cm}^2$ for **3**. These values are 1 order of magnitude higher than the values reported for inorganic crystalline and amorphous materials.^{31,32,36,37} The higher stimulated emission cross-section results from the lower effective bandwidths compared to amorphous materials where they are in the range of 60–80 nm. The narrow bandwidth and high stimulated emission cross sections facilitates the application of these materials for high gain optical amplifiers.

C–H (2950 cm^{-1}) functional groups are potential quenchers of near-infrared emission in many coordination compounds. The second order C–H overtones are almost in resonance with the 1.4 and 1.7 μm emissions, respectively, and hence can contribute to the efficient nonradiative deactivation of the $^3\text{H}_4$ and $^3\text{F}_4$ levels. In the present compounds C–H is present, but in an apparently limited sense, bound to weakly coordinated neutral donor ligands rather than anions, and separated by at least three (Ln–O–C–H) bonds. The number of C–H bonds where the H is separated from Tm by three bonds is 20/Tm in **1**, 10/Tm in **2**, and 6/Tm in **3**, which clearly indicates that the number of proximate CH bonds is not the sole factor influencing NIR intensity.

Concentration quenching is the other factor that has been shown to influence emission intensity in chalcogenide based Ln compounds. There is no significant quenching expected for monometallic **1**, where nearest Tm–Tm neighbors in the

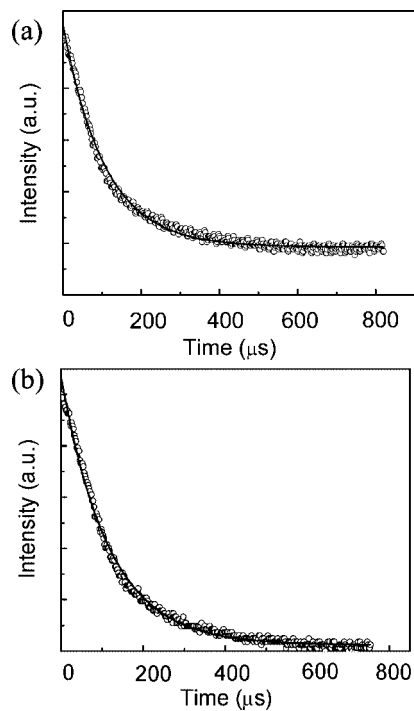


Figure 7. Fluorescence decay curves of the (a) 1.4 and (b) 1.7 μm emissions in $(\text{THF})_6\text{Tm}_4\text{Se}_9(\text{SeC}_6\text{F}_5)_2$.

crystal lattice are at least 8.50 \AA . However, polymetallic **2** and **3** have nearest neighbors within 4.1 \AA , and of these, the linear cluster compound **3** has twice as many of these close Tm–Tm separations. That **2** has the greatest quantum efficiency of **1**–**3** can thus be attributed to a combination fewer C–H bonds relative to **1** and fewer Tm–Tm interactions relative to **3**.

With direct coordination of Tm^{3+} to heavier atoms, the coupling between the energy levels is less efficient and the Franck–Condon factor for the relaxation process is reduced, effectively increasing the lifetime. Thus, all compounds are highly emissive in the near-IR spectrum, particularly when compared to the current literature.

Absolute relationships that correlate structure and fluorescence spectral properties are still elusive. By proper energy transfer and crystal field modeling even though it is possible to design the structure for the best performance, the experimental realization of such systems is difficult due to chemical and thermodynamic stability requirements that control the phase formation of the system. In the present Tm experiments, the tetrametallic compound $(\text{DME})_4\text{Tm}_4(\text{SPh})_{12}$ is shown to be the most emissive Tm compound reported to date.

Conclusion

Thiolate complexes of Tm(III) are highly NIR emissive because of the low phonon energy provided by heavy chalcogen-based anions, with 2–11% quantum yields of NIR emission, which is considered to be the highest reported value for a molecular Tm emission. Fluorination of the thiolate does not appreciably increase quantum efficiency, which is found to be more heavily dependent upon the frequency of proximate C–H bonds and concentration quenching effects.

(36) CanoTorres, J. M.; Serrano, M. D.; Zaldo, C.; Rico, M.; Mateos, X.; Liu, J.; Griebner, U.; Petrov, V.; Valle, F. J.; Galan, M.; Viera, G. J. *Opt. Soc. Am. B* **2006**, *25*, 2594, 23.

(37) Balda, R.; Lacha, L. M.; Fernandez, J. M.; Fernandez-Navarro, J. M. *Proc. SPIE* **2005**, *5723*, 55.

The strong emission characteristics of these compounds suggest that they are potentially useful candidate of 1.4 μm emission in active optical devices where high quantum efficiency is a prerequisite for effective optical amplification.

Acknowledgment. This material is based upon work supported by the National Science Foundation under CHE-0747165. R.R. and G.A.K. acknowledge the New Jersey State Commission on Science and Technology and USR Optonix for their

generous support.

Supporting Information Available: Crystal data and structure refinement, atomic coordinated and equivalent isotropic displacement parameters, bond lengths and angles, anisotropic displacement parameters, and torsion angles for **1** and **2** (as text files). This material is available free of charge via the Internet at <http://pubs.acs.org>.

CM800627F